Blind Noisy Image Deblurring Using Residual Guidance Strategy

Supplementary Material

1. Overview

In this supplemental material, we provide extended experimental results to illustrate the superiority of the proposed method. The supplementary material is organized as follows. In Sec. 2, we present more visual comparisons of images with different kernels from the Lai *et al*. dataset [7], Realblur dataset [13], Levin *et al*. dataset [9] and Kohler *et al*. dateset [5]. In Sec. 3, we illustrate the visual comparisons of other methods with and without our proposed residual guidance strategy on different datasets. In Sec. 4, we give more visual comparison results for different guiding strategies: NGS and RGS. In Sec. 5, we present some results of ablation studies.

2. Additional Visual Comparison Results

We compare our method with Zhong *et al*. [15], Dong *et al*. [3], Li *et al*. [10], Anger *et al*. [1], Selfdeblur [12], VDIP [4], Zhang *et al*. [14], Lee *et al*. [8], WDIP [2], DeblurGAN-v2 [6] on different datasets. Here we provide the comparative results not included in the main text. Notice that, to ensure fairness, except for end-to-end approaches [6, 14], we use the same non-blind deblurring method proposed in [15] after estimating the blur kernel.

2.1. Lai *et al*. dataset

Figs. 1 to 4 display the comparison results on the different types of the Lai *et al*. dataset [7]. It is apparent that other methods struggle to accurately estimate the blur kernel shape, leading to numerous ringing artifacts and noise in the restored results. However, the proposed method achieves an accurate estimated kernel, recovers substantial details, and minimizes artifacts effectively.

2.2. Realblur dataset

In Fig. 5, we compare our method with state-of-the-art methods on the Realblur dataset [13]. It is evident that our method outperforms others [1, 3, 4, 6, 10, 12, 14] in effectively removing blur and providing more accurate blur kernel estimation under noise of $\sigma = 0.1$. In contrast, ringing artifacts and noise are presented in the results of other methods.

2.3. Levin *et al*. dataset

Fig. 6 shows a comparative example on Levin *et al*. [9]. Our method demonstrates the ability to recover a kernel that closely approximates the ground truth, resulting in a sharper and more accurate deblurring outcome. In contrast, the outputs of others continue to display noticeable noise and blur.

2.4. Kohler *et al*. dataset

Tab. 1 show the qualitative and quantitative results of different methods on the Kohler *et al*. [5] dataset. It is clear that our method outperforms other methods [4, 8, 12].

Table 1. Quantitative evaluation of different methods on the Kohler dataset with $\sigma = 0.1$.

Method	PSNR ↑	SSIM ↑	LPIPS ↓
SelfDeblur [12]	13.9	0.21	0.64
Lee *et al*. [8]	22.5	0.62	0.28
VDIP [4]	12.46	0.12	0.61
Ours	**24.94**	**0.70**	**0.27**

3. Extension to other method

The proposed multi-scale residual guidance strategy (RGS) is highly adaptable and can be integrated with other methods, taking [3] as an example. Dong *et al*. [3] addressed blind image deblurring with outliers by proposing a method that mitigates their impact on blur kernel estimation without relying on heuristic detection steps. Fig. 7 illustrates a saturated blurred image with $\sigma = 0.1$, which can be seen as a degraded image with a lot of outliers. However, the method [3] fails to estimate the blur kernel accurately due to the existence of noise. With the assistance of RGS, the accuracy of the estimated kernel is significantly enhanced, effectively eliminating blur. Similarly, Figs. 8 to 10 illustrate the comparative effects of [3] before and after applying the RGS on the Lai *et al*. [7], Levin *et al*. [9], and RealBlur [13] datasets, respectively. These plots provide a more intuitive demonstration of how the proposed strategy enhances the robustness of other methods against high level of noise.

4. Effectiveness of residual guidance strategy

We present additional comparative results for the two guidance strategies, NGS and RGS, as illustrated in Figs. 7 to 10. For instance, incorporating the NGS produces relatively more precise kernels with enhanced detail recovery compared to the method [3]. Additionally, applying the RGS to [3] yields a more superior outcome than the NGS, both in terms of kernel estimation and final deconvolution result. Remarkably, it can be seen that our approach leads to optimal results. This is because our method builds upon Liu *et al*. [11], which introduces an excellent surface-aware prior that effectively suppresses undesirable artifacts.

5. Ablation study

5.1. The number of scales

Our method is implemented within an image pyramid framework. Specifically, the number of pyramid layers is adaptively determined based on the kernel size. To investigate the impact of scale settings on the proposed RGS, we compare three configurations: a fixed number of layers (3 and 5), and our adaptive strategy on the Lai *et al*. dataset with noise level of $\sigma = 0.1$. Tab. 2 presents the corresponding results for PSNR, SSIM, and MNC under different scale settings. Our adaptive parameterization consistently demonstrates superior performance across all evaluation metrics.

Table 2. Impact of different scale settings of the proposed RGS.

Numbers	PSNR ↑	SSIM ↑	MNC ↓
3 scales	19.15	0.57	0.63
5 scales	19.91	0.62	0.71
Adaptive (ours)	**21.41**	**0.75**	**0.77**

5.2. Algorithmic efficiency

We also compare the average inference time of different methods on the Lai *et al*. dataset. Tab. 3 shows that, despite being a traditional algorithm, our method outperforms some learning-based approaches in inference time.

Table 3. Average inference time of different methods on the Lai dataset with $\sigma = 0.1$.

Method	Time (s)
SelfDeblur [12]	757.56
VDIP [4]	605.43
WDIP [2]	10181.98
Lee *et al*. [8]	315.20
Ours	**145.51**

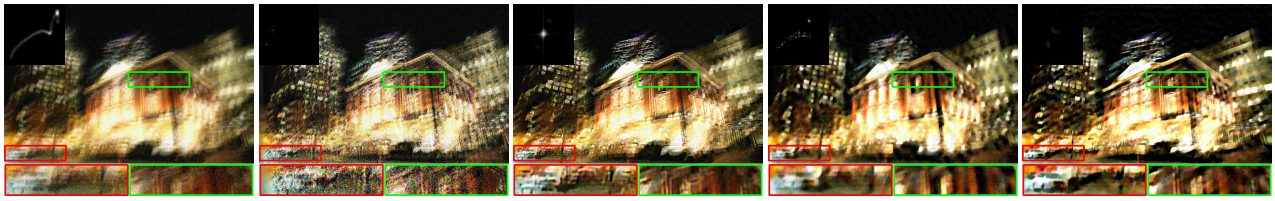

(a) Degraded image (b) WDIP [2] (c) Lee *et al*. [8] (d) Li *et al*. [10] (e) Anger *et al*. [1]

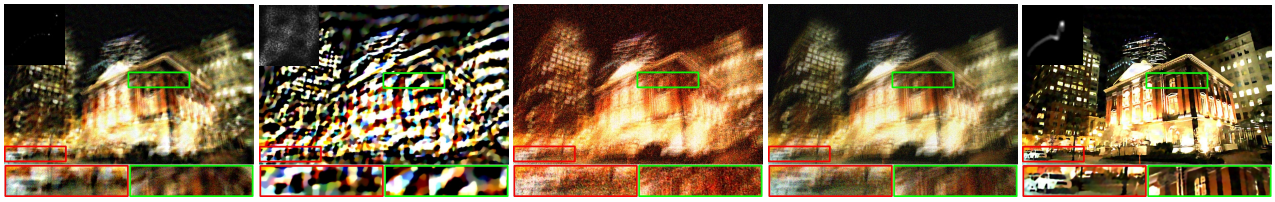

(f) SelfDeblur [12] (g) VDIP [4] (h) Zhang *et al*. [14] (i) DeblurGAN-v2 [6] (j) Ours

Figure 1. Visual comparisons of different deblurring methods of the saturated type on Lai *et al*. dataset [7] with noise level of $\sigma = 0.1$.

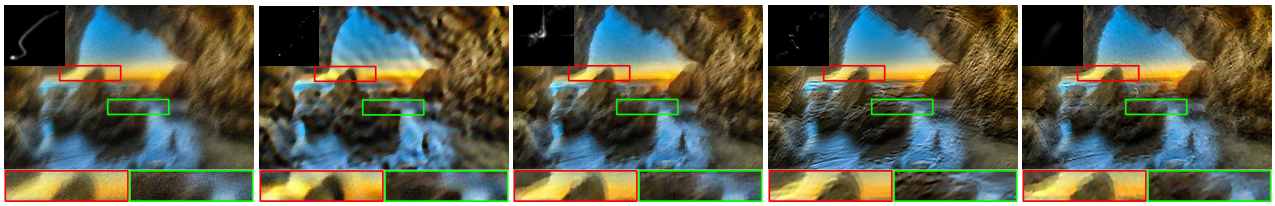

(a) Degraded image (b) WDIP [2] (c) Lee *et al*. [8] (d) Li *et al*. [10] (e) Anger *et al*. [1]

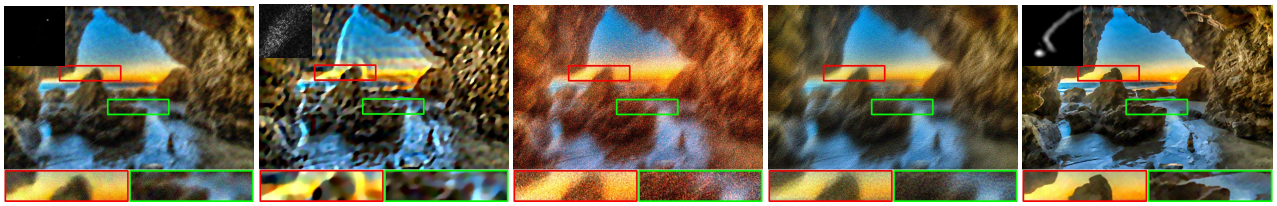

(f) SelfDeblur [12] (g) VDIP [4] (h) Zhang *et al*. [14] (i) DeblurGAN-v2 [6] (j) Ours

Figure 2. Visual comparisons of different deblurring methods of the natural type on Lai *et al*. dataset [7] with a noise level of $\sigma = 0.1$.

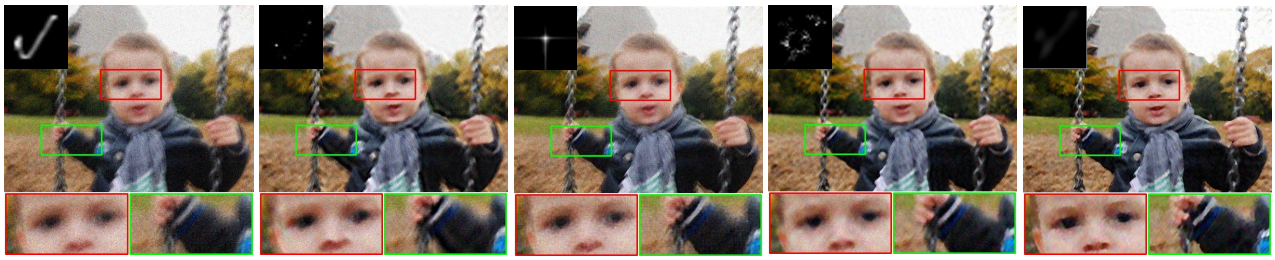

(a) Degraded image (b) WDIP [2] (c) Lee *et al*. [8] (d) Li *et al*. [10] (e) Anger *et al*. [1]

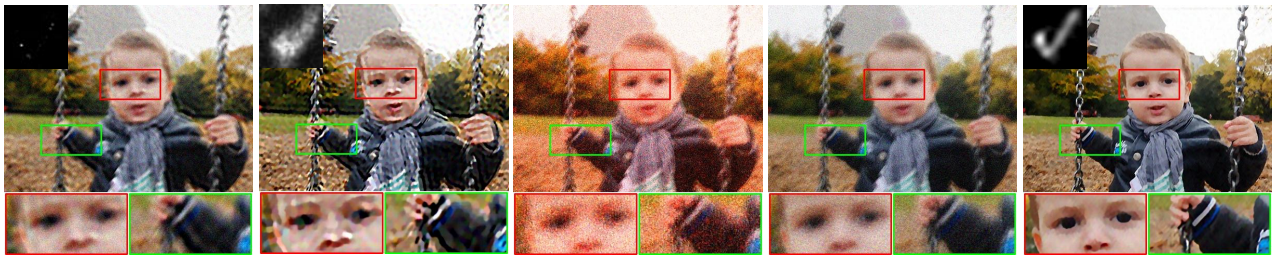

(f) SelfDeblur [12] (g) VDIP [4] (h) Zhang *et al*. [14] (i) DeblurGAN-v2 [6] (j) Ours

Figure 3. Visual comparisons of different deblurring methods of the people type on Lai *et al*. dataset [7] with a noise level of $\sigma = 0.1$.

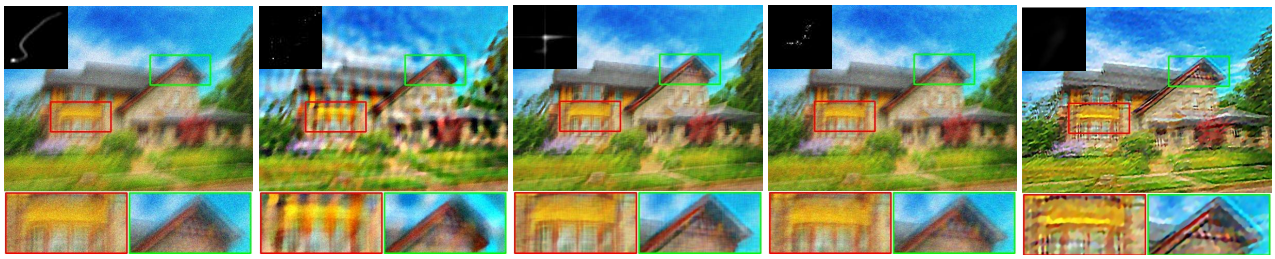

(a) Degraded image (b) WDIP [2] (c) Lee *et al*. [8] (d) Li *et al*. [10] (e) Anger *et al*. [1]

(f) SelfDeblur [12] (g) VDIP [4] (h) Zhang *et al*. [14] (i) DeblurGAN-v2 [6] (j) Ours

Figure 4. Visual comparisons of different deblurring methods of the manmade type on Lai *et al*. dataset [7] with noise level of $\sigma = 0.1$.

(a) Degraded image (b) Dong *et al*. [3] (c) Li *et al*. [10]

(d) Anger *et al*. [1] (e) SelfDeblur [12] (f) VDIP [4]

(g) Zhang *et al*. [14] (h) DeblurGAN-v2 [6] (i) Ours

Figure 5. Visual comparisons of different deblurring methods on the Realblur dataset [13] with noise level of $\sigma = 0.1$.

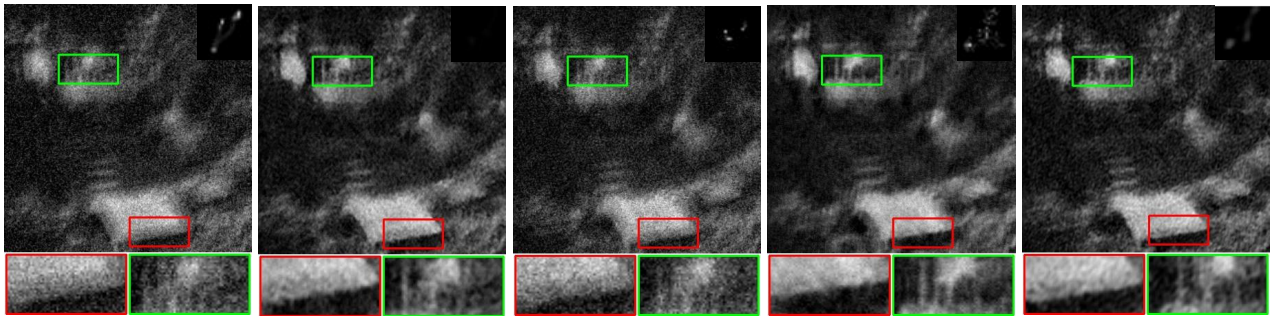

(a) Degraded image (b) Zhong *et al*. [15] (c) Dong *et al*. [3] (d) Li *et al*. [10] (e) Anger *et al*. [1]

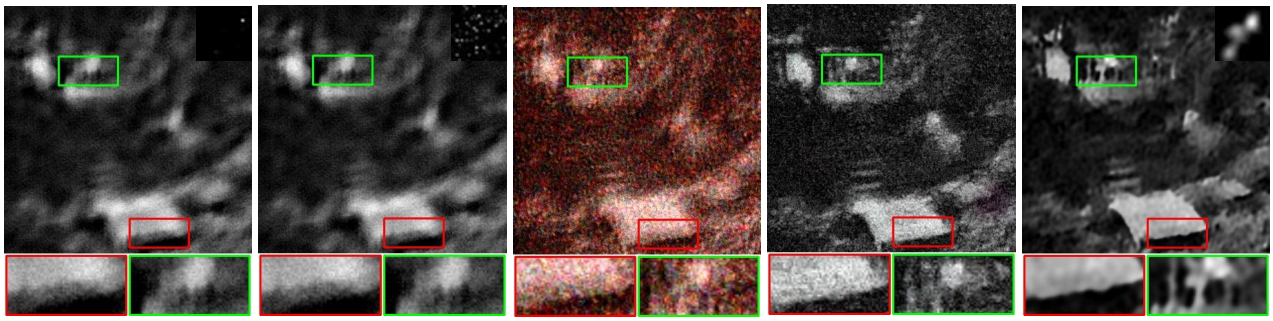

(f) SelfDeblur [12] (g) VDIP [4] (h) Zhang *et al*. [14] (i) DeblurGAN-v2 [6] (j) Ours

Figure 6. Visual comparisons of different deblurring methods on the Levin *et al*. [9] dataset with a noise level of $\sigma = 0.1$.

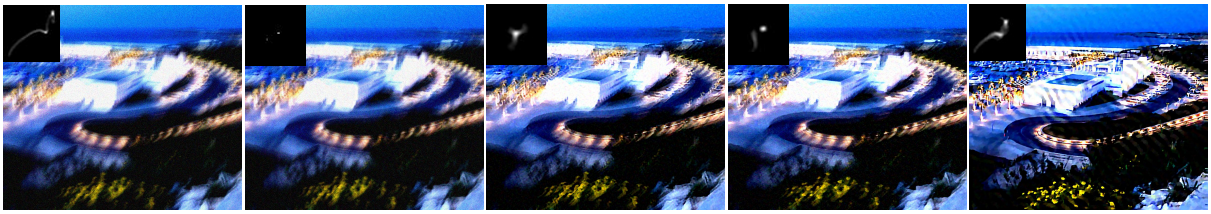

(a) Degraded image (b) Dong *et al*. [3] (c) Dong *et al*. [3] + NGS (d) Dong *et al*. [3] + RGS (e) Ours

Figure 7. Visual comparisons of different guiding strategies on the Lai *et al*. [7] dataset with a noise level of $\sigma = 0.1$.

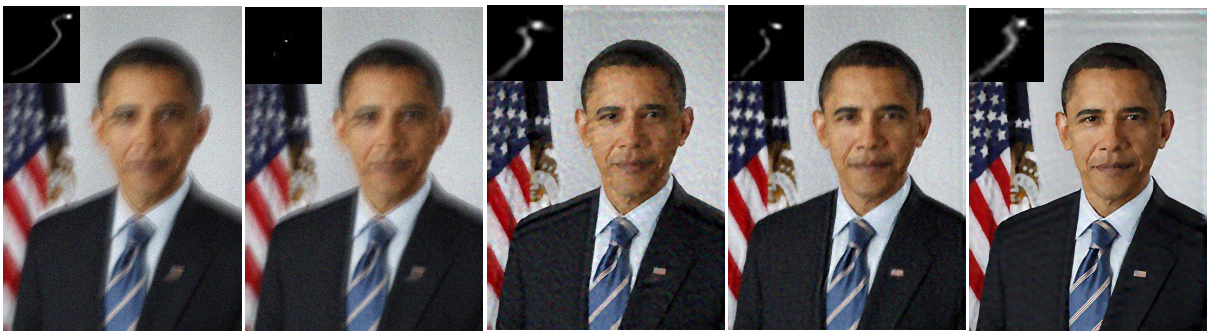

(a) Degraded image (b) Dong *et al*. [3] (c) Dong *et al*. [3] + NGS (d) Dong *et al*. [3] + RGS (e) Ours

Figure 8. Visual comparisons of different guiding strategies on the people type of the Lai *et al*. [7] dataset with a noise level of $\sigma = 0.1$.

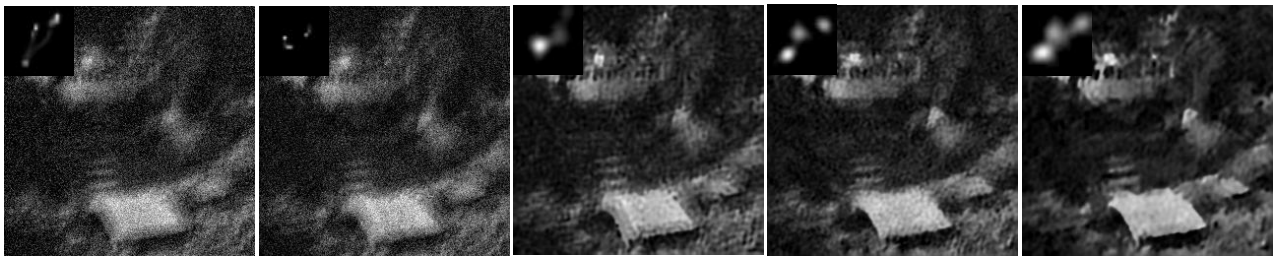

(a) Degraded image (b) Dong *et al*. [3] (c) Dong *et al*. [3] + NGS (d) Dong *et al*. [3] + RGS (e) Ours

Figure 9. Visual comparisons of different guiding strategies on Levin *et al*. [9] dataset with a noise level of $\sigma = 0.1$.

(a) Degraded image (b) Dong *et al*. [3] (c) Dong *et al*. [3] + NGS (d) Dong *et al*. [3] + RGS (e) Ours

Figure 10. Visual comparisons of different guiding strategies on Realblur dataset [13] with a noise level of $\sigma = 0.1$.

References

[1] Jérémy Anger, Mauricio Delbracio, and Gabriele Facciolo. Efficient blind deblurring under high noise levels. In *ISPA*, pages 123–128, 2019. 2, 4, 5, 6, 7

[2] Gustav Bredell, Ertunc Erdil, Bruno Weber, and Ender Konukoglu. Wiener guided dip for unsupervised blind image deconvolution. In *ICCV*, pages 3047–3056, 2023. 2, 3, 4, 5

[3] Jiangxin Dong, Jinshan Pan, Zhixun Su, and Ming-Hsuan Yang. Blind image deblurring with outlier handling. In *ICCV*, pages 2478–2486, 2017. 2, 6, 7, 8

[4] Dong Huo, Abbas Masoumzadeh, Rafsanjany Kushol, and Yee-Hong Yang. Blind image deconvolution using variational deep image prior. *PAMI*, 45(10):11472–11483, 2023. 2, 3, 4, 5, 6, 7

[5] Rolf Köhler, Michael Hirsch, Betty Mohler, Bernhard Schölkopf, and Stefan Harmeling. Recording and playback of camera shake: Benchmarking blind deconvolution with a real-world database. In *ECCV*, pages 27–40. Springer, 2012. 2

[6] Orest Kupyn, Tetiana Martyniuk, Junru Wu, and Zhangyang Wang. Deblurgan-v2: Deblurring (orders-of-magnitude) faster and better. In *ICCV*, pages 8878–8887, 2019. 2, 4, 5, 6, 7

[7] Wei-Sheng Lai, Jia-Bin Huang, Zhe Hu, Narendra Ahuja, and Ming-Hsuan Yang. A comparative study for single image blind deblurring. In *CVPR*, pages 1701–1709, 2016. 2, 4, 5, 7

[8] Chanseok Lee, Jeongsol Kim, Seungmin Lee, Jaehwang Jung, Yunje Cho, Taejoong Kim, Taeyong Jo, Myungjun Lee, and Mooseok Jang. Blind image deblurring with noise-robust kernel estimation. In *ECCV*, pages 188–204. Springer, 2024. 2, 3, 4, 5

[9] Anat Levin, Yair Weiss, Fredo Durand, and William T Freeman. Understanding blind deconvolution algorithms. *PAMI*, 33(12):2354–2367, 2011. 2, 7, 8

[10] Juncheng Li, Faming Fang, Kangfu Mei, and Guixu Zhang. Multi-scale residual network for image super-resolution. In *ECCV*, 2018. 2, 4, 5, 6, 7

[11] Jun Liu, Ming Yan, and Tieyong Zeng. Surface-aware blind image deblurring. *PAMI*, 43(3):1041–1055, 2019. 2

[12] Dongwei Ren, Kai Zhang, Qilong Wang, Qinghua Hu, and Wangmeng Zuo. Neural blind deconvolution using deep priors. In *CVPR*, pages 3341–3350, 2020. 2, 3, 4, 5, 6, 7

[13] Jaesung Rim, Haeyun Lee, Jucheol Won, and Sunghyun Cho. Real-world blur dataset for learning and benchmarking deblurring algorithms. In *ECCV*, pages 184–201, 2020. 2, 6, 8

[14] Kaihao Zhang, Wenhan Luo, Yiran Zhong, Lin Ma, Bjorn Stenger, Wei Liu, and Hongdong Li. Deblurring by realistic blurring. In *CVPR*, pages 2737–2746, 2020. 2, 4, 5, 6, 7

[15] Lin Zhong, Sunghyun Cho, Dimitris Metaxas, Sylvain Paris, and Jue Wang. Handling noise in single image deblurring using directional filters. In *CVPR*, pages 612–619, 2013. 2, 7